

## Stretch-Induced Bending of Soft Ribbed Strips

Emmanuel Siéfert<sup>\*</sup>*Nonlinear Physical Chemistry Unit, Université Libre de Bruxelles, B-1050 Bruxelles, Belgium*Nicolas Cattaud, Etienne Reyssat<sup>†</sup>, Benoît Roman<sup>‡</sup>, and José Bico<sup>§</sup>*Laboratoire de Physique et Mécanique des Milieux Hétérogènes, CNRS, ESPCI Paris, Université PSL, Sorbonne Université, Université de Paris, F-75005 Paris, France* (Received 8 April 2021; revised 1 July 2021; accepted 31 August 2021; published 14 October 2021)

We show that ribbed elastic strips under tension present large spontaneous curvature and may close into tubes. In this single material architected system, transverse bending results from a bilayer effect induced by Poisson contraction as the textured ribbon is stretched. Surprisingly, the induced curvature may reverse if ribs of different orientations are considered. Slender ribbed structures may also undergo a nontrivial buckling transition. We use analytical calculations to describe the evolution of the morphology of the ribbon and the transitions between the different experimental regimes as a function of material properties, geometrical parameters, and stretching strain. This scale-independent phenomenon may help the manufacturing of tubular textured structures or easily controllable grippers at small scale.

DOI: 10.1103/PhysRevLett.127.168002

Textures on soft surfaces are ubiquitous in both natural and manmade systems. They grant enhanced chemical properties to the surfaces, such as wetting [1] and adhesion [2–4], produce structural colors [5], or provide control on tribology [6,7]. Such textures are, however, prone to buckle and to crease when the substrate is submitted to stress [8–10]. Although generally undesired, such morphological instabilities have been harnessed for micropatterning [11], mechanical characterization [12], or design of flexible electronics [13]. Here, we show that rib structures on a strip made of a single material lead to significant transverse bending upon stretching. The orientation and the magnitude of the induced curvature surprisingly depends on the orientation of the ribs. These simple structures may thus be viewed as examples of flexible metamaterials [14], i.e., structures in which microarchitecture induces unconventional properties through simple traction and/or compression (e.g., twist [15], textures [16], or transverse curvature [17]).

Common strategies for programming the bending of a slender structure rely on combining two layers of different materials into a bilayer. The layers react with different expansion or swelling to a given stimulus (e.g., humidity for pine cones [18] or hygromorph structures [19–21], temperature for thermostats [22], interdiffusion for silicon polymers [23]), inducing a length mismatch between both layers. As the layers are assembled together, a stress gradient is generated across the thickness and the structure spontaneously bends, the longer layer being at the outer part of the structure. Bilayer effects have been intensively studied since the pioneering works of Stoney [24] and Timoshenko [22]. They are, for instance, essential in recently developed technologies such as soft robotics grippers [25–28].

Here, we introduce a simple strategy to produce controllable curvature by stretching soft textured ribbons. Rubber ribbons are patterned with transverse walls of the same material (Fig. 1). The key point is that, upon

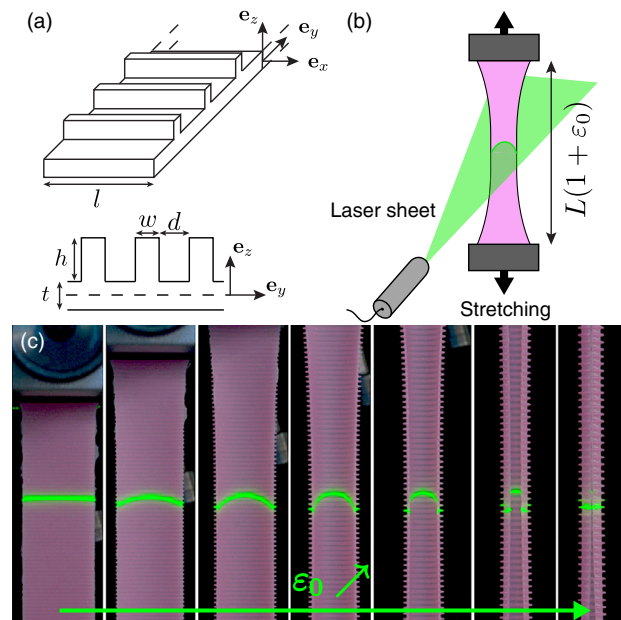


FIG. 1. Stretching of textured ribbons. (a) Sketch of a portion of the ribbon of width  $l$  (top). Cross section of the corrugated ribbed strip with membrane thickness  $t$ , walls of height  $h$  and width  $w$  separated by distance  $d$  (bottom). (b) Experimental setup: a laser sheet intercepts the ribbon (stretched along the  $e_y$  direction) in order to measure its curvature. (c) Ribbon with increasing imposed strain  $\epsilon_0$ : the ribbon progressively bends along its transverse direction and eventually rolls itself into a tube.

traction, the width of the ribbon decreases by Poisson effect, whereas the walls, oriented perpendicularly to the traction direction, are barely affected by the stretching of the membrane on which they sit. The resulting mismatch in width induces an effective bilayer effect, and the ribbon rolls itself into a tubular shape whose curvature increases with the imposed strain  $\varepsilon_0$  (Fig. 1(c) here and Movie 1 in the Supplemental Material [29]).

We first focus on walls oriented normally to the traction direction. Adapting Timoshenko's reasoning, we obtain an analytical prediction in the linear regime and compare it with our experiments over a wide range of geometrical parameters. We deduce the optimal size and density of the walls on a ribbon of a given thickness, providing the maximum curvature-over-stretch ratio. We then extend the theory to tilted walls and predict the surprising inversion of the induced curvature for a critical inclination angle. We finally observe that walls may buckle as the ribbon is stretched; we describe compressive stresses in the texture and derive analytically the onset of buckling of the ribs.

The textured strips are made of silicone elastomers (Elite Double 8 or 22 from Zhermack, Dragonskin 10 from Smooth-On) by mixing equal quantities of *catalyst* and *base* liquids. The mixture is then poured into a 3D printed mold with the desired geometric parameters. After curing, the ribbon has a rest length  $L$ , a width  $l$ , and a base thickness  $t$  with  $L \gg l \gg t$ . It is textured with walls of height  $h$  and thickness  $w$ . The walls are regularly spaced by a distance  $d$  and are oriented perpendicularly to the ribbon direction [Fig. 1(a)]. We define the density of textures as  $\phi = w/(d + w)$ . The ribbon is clamped into a traction test machine and stretched to a strain  $\varepsilon_0 = \Delta L/L$  [Fig. 1(b)]. The curvature of the ribbon is measured far from the fixed ends of the ribbon, shining a laser sheet with an oblique incidence. The deflections of the laser line are proportional to the local out-of-plane displacements of the ribbon (see the Supplemental Material [29]).

To rationalize the transverse bending observed upon stretching (Fig. 1(c) here and Movie 1 in the Supplemental Material [29]), we make the following simplifying assumptions: (i) the boundary layer over which the base of the walls is stretched by the substrate is small compared to the height of the walls and can thus be neglected (i.e.,  $h \gg w$ ), (ii) the base of the ribbon is stretched homogeneously with a strain  $\varepsilon_0$  despite the local reinforcements induced by the presence of the walls (this assumption is valid when  $t \gg w$ ), and (iii) the walls are sufficiently close to one another to avoid any significant curvature difference between the portions of the ribbon covered or not by a wall. We consider a homogenized version of the membrane composed of a first layer (the base of the ribbon) stretched with a strain  $\varepsilon_0$  and a second layer (the walls) that is unstretched. Stretching the first layer induces a transverse contraction that compresses the second layer in the direction normal to the applied traction. The curvature and the

position of the neutral plane can be derived by minimizing the elastic energy in this textured ribbon with respect to these two unknowns (see the Supplemental Material [29]). Within the linear framework of Hookean elasticity, we obtain the following expressions for the normalized curvature  $\tilde{\kappa} = \kappa t$  and the transverse strain  $\xi = \varepsilon_{xx}(z = 0)$  at the membrane midsurface:

$$\tilde{\kappa} = \frac{6\tilde{h}(\tilde{h} + 1)\phi}{1 + 4\tilde{h}\phi + 6\tilde{h}^2\phi + 4\tilde{h}^3\phi + \tilde{h}^4\phi^2} \nu \varepsilon_0, \quad (1)$$

$$\xi = -\frac{1 + 3\tilde{h}\phi + 6\tilde{h}^2\phi + 4\tilde{h}^3\phi}{1 + 4\tilde{h}\phi + 6\tilde{h}^2\phi + 4\tilde{h}^3\phi + \tilde{h}^4\phi^2} \nu \varepsilon_0, \quad (2)$$

where  $\nu$  is the Poisson ratio of the elastomer ( $\nu = 1/2$  throughout this article) and  $\tilde{h} = h/t$  is the dimensionless wall height. The equation for the curvature is equivalent to Timoshenko's formula for bilayers [22], where the wall density  $\phi$  replaces the ratio of Young moduli in both layers. The exact same equations may be derived using classical laminate theory [30], considering the membrane as an isotropic layer and the walls as another orthotropic layer transmitting stresses and loads only in the direction of the walls (see the Supplemental Material [29]). Figure 2(a) shows that the measured curvature varies linearly with the applied strain  $\varepsilon_0$ , in agreement with the model. The curvature of the ribbon may thus be easily controlled by adjusting the amount of stretching. Our theoretical prediction matches quantitatively the measured curvatures, as shown in Fig. 2(b), even for large strains, beyond the limit of validity of the theory. In Fig. 2(c),  $\tilde{\kappa}/\varepsilon_0$  is plotted as a function of the two relevant geometrical parameters  $\phi$  and  $\tilde{h}$ . Maximizing this ratio, we obtain the optimal geometry of the textures ( $\tilde{h} \rightarrow 1/2, \phi \rightarrow 1$ ), which corresponds to a ribbon of thickness  $h + t$  with regularly spaced cuts of depth  $h$ . Such an ideal configuration is however more challenging to manufacture and may be prone to rupture due to stress singularities at the tip of the slits (see a near optimal design ( $\tilde{h} = 1/2, \phi = 0.88$ ) in Fig. S3 in the Supplemental Material [29]). For a more moderate wall density of  $\phi = 1/2$ , experimental measurements of stretch-induced curvature match quantitatively the theoretical prediction [Fig. 2(d)]. We interpret the small overestimation of the curvature as a consequence of the stretching of the base of the walls, which has been neglected in our idealized model. This effect is more pronounced when the aspect ratio of the walls  $h/w$  is small [light green dots in Figs. 2(a) and 2(b)]. More generally, the optimal dimensionless height  $\tilde{h}$  for a given density  $\phi$  reads

$$\phi(\tilde{h}) = 1/[\tilde{h}^2(2\tilde{h} + 3)], \quad (3)$$

represented by the solid black line in Fig. 2(c).

When the walls are not oriented along the width of the ribbon but tilted by an increasing angle  $\chi_0$  (Fig. 3 here and

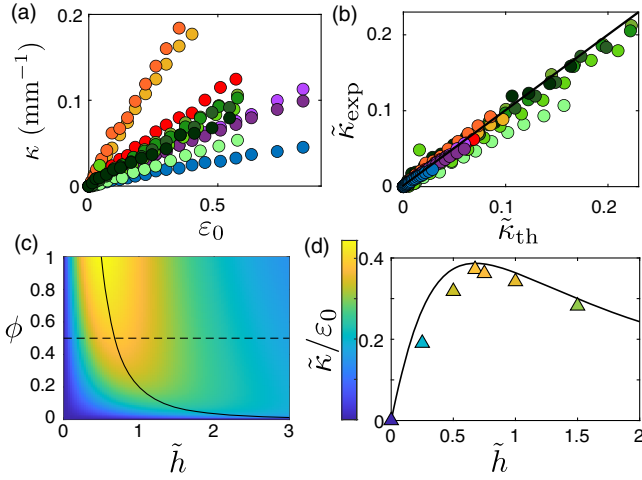


FIG. 2. Stretch-induced curvature. (a) Curvature  $\kappa$  as a function of the imposed strain  $\varepsilon_0$  for various strip geometries. Green dots:  $t = 2$  mm; wall density  $\phi = 1/2$ ;  $w = 0.75$  mm;  $0.5$  mm  $\leq h < 3$  mm;  $0 \leq \varepsilon_0 \leq 0.6$ . Yellow to blue dots:  $t = 0.5$  mm; wall density  $\phi = 1/2$ ;  $0.5$  mm  $\leq w \leq 1$  mm;  $1$  mm  $\leq h \leq 5$  mm;  $0 \leq \varepsilon_0 \leq 0.9$ . The ribbons are made indifferently of two different silicone elastomers (Elite Double 8 and 22 from Zhermack) of respective Young's modulus  $E = 250$  kPa and  $E = 650$  kPa, and Poisson ratio  $\nu = 0.5$ . (b) Experimental versus theoretical dimensionless curvature  $\tilde{\kappa} = \kappa t$ . (c) Curvature-over-strain ratio  $\tilde{\kappa}/\varepsilon_0$  [color with scale given by the ordinate axis in plot (d)] as a function of the relative wall height  $\tilde{h} = h/t$  and wall density  $\phi = w/(d+w)$ . The full line corresponds to the optimal value of  $\tilde{h}$  as a function of  $\phi$ . (d) Curvature-over-strain ratio as a function of  $\tilde{h}$  for  $\phi = 0.5$  [dashed line in (c)]. Triangles are obtained by a linear fit of the experimental curves  $\kappa = f(\varepsilon_0)$  and the black line is the theory (Eq. (1)).

Movie 2 in the Supplemental Material [29]), we observe that the curvature-over-stretch ratio decreases and eventually reverses above a critical tilting angle  $\chi_c \approx 35^\circ$ . This surprising feature commands an extended analytical treatment. Qualitatively, stretching a smooth ribbon with a strain  $\varepsilon_0$  induces a transverse contraction  $-\nu\varepsilon_0$ . Hence, a tilted material line making an initial angle  $\chi_0$  with the width direction has a length  $\ell_0 = l/\cos\chi_0$  before stretching and  $\ell = \ell_0 \sqrt{\cos^2\chi_0(1-\nu\varepsilon_0)^2 + \sin^2\chi_0(1+\varepsilon_0)^2}$  after stretching. The strain experienced by this material line thus reads  $\varepsilon_\ell = \cos^2\chi_0(\tan^2\chi_0 - \nu)\varepsilon_0$  to the first order in  $\varepsilon_0$ . This strain vanishes for a specific orientation of the line  $\chi_c = \arctan\sqrt{\nu} \approx 35^\circ$ . When  $\chi_0 < \chi_c$  (respectively,  $\chi_0 > \chi_c$ ), the line contracts (respectively, expands). Considering now a wall on this tilted line, contraction ( $\chi_0 < \chi_c$ ) induces a curvature with the walls on the outside, whereas elongation ( $\chi_0 > \chi_c$ ) leads to the curvature of the structure with the walls on the inside, as observed experimentally (Fig. 3 here and Movie 2 in the Supplemental Material [29]).

Quantitatively, bending of the ribbon not only induces bending of the wall but also twist. For the sake of simplicity, we neglect the corresponding twisting energy since the torsion constant  $J \sim hw^3$  of the wall is much

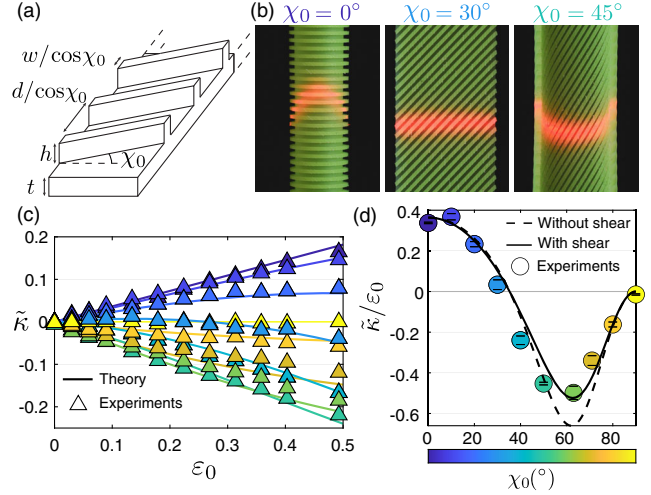


FIG. 3. Varying the wall orientation. (a) Ribbon with walls tilted by an angle  $\chi_0$ . (b) Stretched ribbons with walls of various orientations  $\chi_0$  and thus different transverse curvature directions. (c) Dimensionless curvature  $\tilde{\kappa}$  as a function of the applied strain  $\varepsilon_0$  for various angles  $\chi_0$  (colors according to the angle  $\chi_0$  with the color bar presented in (d);  $h = 1$  mm;  $t = 1$  mm;  $d = w = 0.28$  mm). Solid lines correspond to the theoretical model with shear [Eq. (5)]. (d) Curvature-over-strain ratio at small strain as a function of  $\chi_0$ . Triangles are obtained by a linear fit of the first 6 experimental points in graph (c). The dashed line is the theoretical prediction [Eq. (4)] of the simplified model neglecting shear. The solid black line corresponds to the full model accounting for shear (see the Supplemental Material [29]). A quantitative agreement is obtained for all angles without any fitting parameter.

smaller than the bending constant  $I \sim h^3w$  in the regime of interest ( $h \gg w$ ). A derivation taking into account the twisting of the wall is presented in the Supplemental Material [29]. More importantly, the membrane may also experience a global shear strain due to the presence of the tilted walls. This additional effect is tackled in the Supplemental Material [29]. Neglecting shear and assuming a cylindrical configuration, the total elastic energy may be computed both in the membrane and in the walls and then minimized with respect to the curvature  $\kappa$  and the transverse strain  $\xi$  of the membrane midsurface in the limit of small strain (see the Supplemental Material [29]). The normalized curvature finally reads as follows:

$$\tilde{\kappa} = \frac{6\tilde{h}(\tilde{h}+1)\phi\cos^4\chi_0(\nu - \tan^2\chi_0)}{\underbrace{1 + \phi\cos^4\chi_0(4\tilde{h} + 6\tilde{h}^2 + 4\tilde{h}^3) + \phi^2\cos^8\chi_0\tilde{h}^4}_{f(\chi_0, \tilde{h}, \phi, \nu)}}\varepsilon_0. \quad (4)$$

When  $\chi_0 = 0$ , we retrieve Eq. (1). As observed in the experiments [Fig. 3(d)], the curvature-over-stretch ratio at small strains vanishes and changes its sign at the specific orientation of the walls  $\chi_c$ . Our simplified model [dashed line in Fig. 3(d)] shows good agreement with the experimental data, except for  $\chi_0 \approx 60^\circ$ . The agreement may be

further improved by taking into account a global shear strain in the membrane (solid line). Classical laminate theory, associated with a rotation of the coarse-grained plane-stress stiffness matrix of the walls, leads to the same result (see the Supplemental Material [29]). Beyond the linear behavior described in Eq. (4), the full nonlinear curvature versus strain curve may be retrieved by updating the actual angle  $\chi$  in the deformed state. Neglecting the shear, this actual angle approximately reads  $\chi(\epsilon_0, \chi_0) = \arctan [(1 + \epsilon_0)/(1 - \nu\epsilon_0) \tan \chi_0]$ . The curvature-strain curve finally reads

$$\tilde{\kappa} = \int_0^{\epsilon_0} f(\chi(\epsilon, \chi_0), \tilde{h}, \phi, \nu) d\epsilon, \quad (5)$$

where the function  $f$  is the linear coefficient relating the dimensionless curvature  $\tilde{\kappa}$  and the strain  $\epsilon_0$  in Eq. (4). This expression is plotted in Fig. 3(c) and shows good agreement with the experimental data, even at large strains. For walls oriented with an angle  $\chi_0 = 30^\circ$ , the curvature changes its signs above the predicted critical strain (Fig. 3(c) here and Movie 2 in the Supplemental Material [29]).

Our theory, however, fails to accurately predict the response of the strips outside the asymptotic regime described above, especially when  $t$  is not large compared to  $w$  (Fig. S5 in the Supplemental Material [29]). Indeed, the physical bond between the membrane and the walls is overlooked in the model, which induces significant local changes in the strain distribution in the membrane. Taking this subtle effect into account would require a numerical analysis, which is beyond the scope of the present work.

Beyond the global transverse bending of the strips, the textures may undergo a buckling transition for certain geometries above a critical strain (Fig. 4 here and Movie 4 in the Supplemental Material [29]) [31]. We focus here on transverse ribs parallel to the  $\mathbf{e}_x$  direction (i.e.,  $\chi_0 = 0$ ). Because of the presence of the stretched membrane, the ribs are under compression and not in a pure bending mode. The transverse strain inside the ribs may be inferred from the combination of Eqs. (1) and (2) and is geometrically given by  $\epsilon_{xx}(z) = \xi + \kappa z$ . The buckling of a thin wall on a compressed foundation—or equivalently, the swelling of a wall on a passive foundation—has been studied in the context of swelling bilayers of gels [32]. Buckling is expected to occur when the compressive strain reaches  $\epsilon_c = -0.87w^2/h^2$ , and the wavelength  $\lambda$  at the onset of instability is found proportional to  $h$ . In the present case, however, the walls are additionally bent, which increases the compression close to their base but reduces the compression on the upper part of the walls. We assume that the wall buckles when the top of the wall reaches the critical compressive strain  $\epsilon_c$ , i.e., when

$$\epsilon_{xx}^{\text{top}} = \nu\epsilon_0 \frac{-1 + 3\tilde{h}^2\phi + 2\tilde{h}^3\phi}{1 + 4\tilde{h}\phi + 6\tilde{h}^2\phi + 4\tilde{h}^3\phi + \tilde{h}^4\phi^2} = \epsilon_c. \quad (6)$$

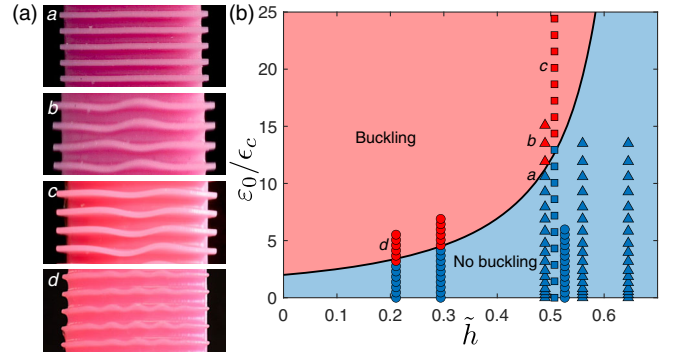


FIG. 4. Wall buckling. (a) Walls for different geometries and stretching  $\epsilon_0$  in a nonbuckling (a) and a buckling (b–d) regime. The lettering corresponds to the lettered symbols in the diagram. (b) Diagram with the rescaled applied strain  $\epsilon_0/\epsilon_c$  as a function of the dimensionless height  $\tilde{h} = h/t$  for  $\phi = 1/2$ . The black lines correspond to the expected buckling threshold [Eq. (6)]. Symbols represent the geometry of the walls: triangles ( $h = 3$  mm;  $w = 0.75$  mm); squares ( $h = 5$  mm;  $w = 1$  mm); circles ( $h = 1$  mm;  $w = 0.5$  mm).

Remarkably, this strain vanishes when the height is optimal for a given density [Eq. (3)]. If the height is larger than the optimum value, the top of the walls is under tension and the structure does not buckle. In the opposite case, the top of the walls is under compression and the compressive strain  $\epsilon_{xx}^{\text{top}}$  increases linearly with  $\epsilon_0$  until it reaches the critical buckling strain  $\epsilon_c$ . Figure 4 shows the configuration diagram with the rescaled strain  $\epsilon_0/\epsilon_c$  as a function of  $\tilde{h}$  for  $\phi = 1/2$ . Our theory predicts quantitatively the transition to buckling for various wall sizes and aspect ratios (Fig. 4). The wavelength of the instability classically scales as  $h$  [32]. When the membrane is infinitely thick (i.e., when  $\tilde{h} \ll 1$ ), we retrieve the classical buckling threshold  $-\nu\epsilon_0 = \epsilon_c$ . As a consequence of buckling, the compressive stresses in the ribs are partially relaxed and the induced bending is less pronounced than predicted in our linear theory [Eq. (1)].

We have demonstrated how spontaneous curvature can be induced by stretching a textured ribbon. This curvature results from the difference in Poisson contraction between the ribbon and the textures and is well described by a simple analytical model. Contrary to standard bilayers, this effect is not caused by a contrast of material properties but by geometry. A natural extension of this work would be to program complex shapes by varying the orientation  $\chi_0$  of the walls along the ribbon. Nevertheless, the gradient of curvature will be limited by a longitudinal persistence length observed when the transverse curvature of a tubular structure is modified [33–35]. Although we focused on macroscale structures, the mechanism is scale-invariant. Many techniques, including soft lithography and two-photon laser writing or etching, are readily available to manufacture textured ribbons at microscales. For micrometer thin structures of 1 mm width, for instance,

a typical strain of a few percent is sufficient to close the ribbon into a cylinder. At small scales, surface stresses should be additionally taken into account [36]. Depending on the orientation of the walls, the obtained tubes may have textures either on the inside or the outside. Such structures could be used for flow control in microfluidic devices or as soft grippers. We therefore envision that the programmable self-curving structures based on surface textures could become a very simple tool to manufacture tubular structures at small scale.

We thank Ido Levin for fruitful discussions and the anonymous reviewer for highly relevant remarks that triggered additional research. E. S. acknowledges funding from the EU's Horizon 2020 research and innovation program under the Individual Marie Skłodowska-Curie fellowship Grant Agreement No. 101027862. This work was partially supported by ANR SMaRT (ANR-15-CE08-0007).

---

\*Corresponding author.  
emmanuel.siefert@ulb.be

- [1] D. Quéré, *Annu. Rev. Mater. Res.* **38**, 71 (2008).
- [2] K. Autumn, M. Sitti, Y. A. Liang, A. M. Peattie, W. R. Hansen, S. Sponberg, T. W. Kenny, R. Fearing, J. N. Israelachvili, and R. J. Full, *Proc. Natl. Acad. Sci. U.S.A.* **99**, 12252 (2002).
- [3] A. K. Geim, S. Dubonos, I. Grigorieva, K. Novoselov, A. Zhukov, and S. Y. Shapoval, *Nat. Mater.* **2**, 461 (2003).
- [4] C. S. Davis, D. Martina, C. Creton, A. Lindner, and A. J. Crosby, *Langmuir* **28**, 14899 (2012).
- [5] Y. Zhao, Z. Xie, H. Gu, C. Zhu, and Z. Gu, *Chem. Soc. Rev.* **41**, 3297 (2012).
- [6] B. Bhushan, *Tribol. Lett.* **4**, 1 (1998).
- [7] E. Wandersman, R. Candelier, G. Debrégeas, and A. Prevost, *Phys. Rev. Lett.* **107**, 164301 (2011).
- [8] C. Lestringant, C. Maurini, A. Lazarus, and B. Audoly, *Phys. Rev. Lett.* **118**, 165501 (2017).
- [9] Y. Zhao, Z.-C. Shao, G.-Y. Li, Y. Zheng, W.-Y. Zhang, B. Li, Y. Cao, and X.-Q. Feng, *Appl. Phys. Lett.* **110**, 231604 (2017).
- [10] A. Takei, F. Brau, B. Roman, and J. Bico, *Europhys. Lett.* **96**, 64001 (2011).
- [11] T. Ohzono, H. Monobe, K. Shiokawa, M. Fujiwara, and Y. Shimizu, *Soft Matter* **5**, 4658 (2009).
- [12] C. M. Stafford, C. Harrison, K. L. Beers, A. Karim, E. J. Amis, M. R. VanLandingham, H.-C. Kim, W. Volksen, R. D. Miller, and E. E. Simonyi, *Nat. Mater.* **3**, 545 (2004).
- [13] Y. Sun, W. M. Choi, H. Jiang, Y. Y. Huang, and J. A. Rogers, *Nat. Nanotechnol.* **1**, 201 (2006).
- [14] K. Bertoldi, V. Vitelli, J. Christensen, and M. Van Hecke, *Nat. Rev. Mater.* **2**, 17066 (2017).
- [15] T. Frenzel, M. Kadic, and M. Wegener, *Science* **358**, 1072 (2017).
- [16] C. Coulais, E. Teomy, K. De Reus, Y. Shokef, and M. Van Hecke, *Nature (London)* **535**, 529 (2016).
- [17] F. Agnelli, M. Tricarico, and A. Constantinescu, *Extreme Mech. Lett.* **42**, 101089 (2021).
- [18] C. Dawson, J. F. Vincent, and A.-M. Rocca, *Nature (London)* **390**, 668 (1997).
- [19] E. Reyssat and L. Mahadevan, *J. R. Soc. Interface* **6**, 951 (2009).
- [20] S. Poppinga, C. Zollfrank, O. Prucker, J. Rühe, A. Menges, T. Cheng, and T. Speck, *Adv. Mater.* **30**, 1703653 (2018).
- [21] Y. Tahouni, T. Cheng, D. Wood, R. Sachse, R. Thierer, M. Bischoff, and A. Menges, in *Proceedings of the Symposium on Computational Fabrication, SCF '20* (Association for Computing Machinery, New York, NY, USA, 2020).
- [22] S. Timoshenko, *J. Opt. Soc. Am.* **11**, 233 (1925).
- [23] M. Pezzulla, G. P. Smith, P. Nardinocchi, and D. P. Holmes, *Soft Matter* **12**, 4435 (2016).
- [24] G. G. Stoney, *Proc. R. Soc. A* **82**, 172 (1909).
- [25] S. Shian, K. Bertoldi, and D. R. Clarke, *Adv. Mater.* **27**, 6814 (2015).
- [26] D. L. DeVoe and A. P. Pisano, *J. Microelectromech. Syst.* **6**, 266 (1997).
- [27] L. Ionov, *Adv. Funct. Mater.* **23**, 4555 (2013).
- [28] R. F. Shepherd, F. Ilievski, W. Choi, S. A. Morin, A. A. Stokes, A. D. Mazzeo, X. Chen, M. Wang, and G. M. Whitesides, *Proc. Natl. Acad. Sci. U.S.A.* **108**, 20400 (2011).
- [29] See Supplemental Material at <http://link.aps.org/supplemental/10.1103/PhysRevLett.127.168002> for additional theoretical and experimental details.
- [30] C. Kassapoglou, *Design and Analysis of Composite Structures* (John Wiley & Sons, New York, 2013).
- [31] H. Lee, J. G. Bae, W. B. Lee, and H. Yoon, *Soft Matter* **13**, 8357 (2017).
- [32] T. Mora and A. Boudaoud, *Eur. Phys. J. E* **20**, 119 (2006).
- [33] L. Mahadevan, A. Vaziri, and M. Das, *Europhys. Lett.* **77**, 40003 (2007).
- [34] T. Barois, L. Tadrist, C. Quilliet, and Y. Forterre, *Phys. Rev. Lett.* **113**, 214301 (2014).
- [35] D. Matsumoto, T. G. Sano, and H. Wada, *Europhys. Lett.* **123**, 14001 (2018).
- [36] J. Zang and F. Liu, *Appl. Phys. Lett.* **92**, 021905 (2008).